ADVANCED OPTICAL MATERIALS
www.advopticalmat.de

An Efficient Perovskite-Like Phosphor with Peak Emission Wavelength at 850 nm for High-Performance NIR LEDs

Wenqiang Tang, Dan Wu, Yu Xiao, Xiaoling Dong, Yue Wang, Wenping Zhou, Yifan Liu, and Liangliang Zhang**

Near-infrared (NIR) phosphor-converted light-emitting diodes (pc-LEDs) are an emerging light source demanded for the miniaturization of NIR spectroscopy. However, the photoelectric efficiency and spectral properties of NIR pc-LEDs are still very limited due to a lack of efficient broadband NIR phosphors with peak emission wavelength >850 nm. Here, a novel Cr^{3+}-activated perovskite-like $Mg_4Ta_2O_9$ phosphor is reported, which exhibits a broad NIR emission band peaking at 850 nm with a high internal (external) quantum efficiency of 72% (33.4%). The fabricated NIR pc-LED shows a broad emission band covering the whole 700–1100 nm spectrum range with a photoelectric conversion efficiency of 22.1% at 10 mA. This work may provide a new paradigm for the discovery of Cr^{3+} singly doped NIR phosphors with excellent performance.

1. Introduction

Near-infrared (NIR) spectroscopy technology is a quantitative analytical method to probe a sample with light in the spectrum range of 700–2500 nm. The mechanism is monitoring fingerprint characteristics absorption of NIR active vibrational modes from heavy atoms such as C, N, O, and S attached to hydrogen.[1–4] Considering the spectrum of the most commonly used Si detector for NIR spectroscopy as well as the penetration in bio-tissues, it is important to develop NIR light sources with a wide enough emission spectrum covering the whole 700–1100 nm range to obtain more effective information in practical application such as food analysis, medical diagnostics, and agricultural science.[5–8] On the other hand, integrating the NIR spectroscopy into mobile phones or wearable devices are emerging demand that call for NIR light source with small size.[9,10] The traditional tungsten-halogen lamps or supercontinuum lasers cannot meet these new applications because of their large size, short lifetime, and poor efficiency.[11,12] NIR light emitting diodes (LEDs) show the advantages of small size, but their emission bandwidth is less than 50 nm, which is too narrow.[13,14] In this context, phosphor-converted LEDs (pc-LEDs) with broad NIR emission were recently proposed, where one or more kinds of NIR phosphors were coated on a blue LED chip. The broad and tunable emission band as well as the small size of such NIR pc-LEDs make them an excellent alternative light source for miniature NIR spectroscopy applications.

The NIR phosphor acts as a key role to convert blue light from LED chip to broadband NIR light.[15] Thus, many efforts have been made to explore NIR phosphors with broad emission band and high efficiency, such as $K_3LuSi_2O_7:Eu^{2+}$ (740 nm),[16] $CaS:Eu^{2+},Tb^{3+}$ (810 nm)[17] and $Lu_2BaAl_4SiO_{12}:Ce^{3+},Mn^{2+}$ (770 nm).[18] The main drawbacks of that Eu^{2+}/Ce^{3+} activated phosphor are their relatively short emission wavelength (<850 nm), low internal quantum efficiency (IQE), and poor thermal stability. Thus, Cr^{3+}-activated NIR phosphors draw more attention for their broad emission bandwidth and high efficiency.[19,20] For example, Song et al. reported $K_2NaScF_6:Cr^{3+}$ NIR phosphor with an emission band peaking at 765 nm and IQE of 74%.[21] Zheng and co-workers designed $Y_2CaAl_4SiO_{12}:Cr^{3+}$ translucent ceramics by cation co-substitution of Ca^{2+}-Si^{4+} for Y^{3+}-Al^{3+} and achieved high IQE (90.1%) and external QE (EQE) (59.5%).[22] Highly efficient NIR emissions have also been reported in other phosphors such as $Ca_2LuHf_2Al_3O_{12}:Cr^{3+}$ (775 nm),[4] $La_2MgZrO_6:Cr^{3+}$ (825 nm),[10] $Ga_2O_3:Cr^{3+}$ (740 nm),[23] $GdAl_3(BO_3)_4:Cr^{3+}$ (733 nm),[24] $LaMgGa_{11}O_{19}:Cr^{3+}$ (770 nm)[25] and so on. Though the above NIR phosphors have high IQE and excellent thermal stability, they also suffer from deficient emission in 850–1100 nm, which limits their practical applications. Some NIR phosphors with longer wavelength emission (>850 nm), such as $La_3Ga_5GeO_{14}:Cr^{3+}$ (920 nm),[26] $ZnTa_2O_6:Cr^{3+}$ (935 nm),[27] and $LiIn_2SbO_6:Cr^{3+}$ (965 nm),[28] were reported, but their IQEs are

W. Tang, D. Wu, X. Dong, Y. Wang, W. Zhou, Y. Liu
School of Physical Science and Technology
Inner Mongolia Key Lab of Nanoscience and Nanotechnology
Inner Mongolia University
Hohhot 010021, P. R. China
E-mail: wudan@imu.edu.cn
Y. Xiao
College of Science
Nanjing Forestry University
Nanjing 210037, P. R. China
L. Zhang
State Key Laboratory of Luminescence and Applications
Changchun Institute of Optics
Fine Mechanics and Physics
Chinese Academy of Sciences
3888 Eastern South Lake Road, Changchun 130033, P. R. China
E-mail: zhangliangliang@ciomp.ac.cn
The ORCID identification number(s) for the author(s) of this article can be found under https://doi.org/10.1002/adom.202202237.

DOI: 10.1002/adom.202202237

relatively low (typically <30%). Overall, developing broadband NIR phosphors with peak emission wavelength >850 nm and high QE remains a meaningful and challenging target.

In this work, a new broadband perovskite-like NIR phosphor $Mg_4Ta_2O_9$ (MTO):Cr^{3+} is reported. The MTO:0.03 Cr^{3+} phosphor has a broad NIR emission band peaking at 850 nm with full-width at half maximum (FWHM) of 188 nm. The IQE and absorption (Abs) are 72% and 46.4%, respectively, which results in an EQE of 33.4% under 460 nm excitation. The NIR pc-LED fabricated by MTO:0.03 Cr^{3+} phosphor shows a NIR emission band covering the whole 700–1100 nm spectrum range. The NIR output power is 5.7 mW@10 mA with a photoelectric conversion efficiency of 22.1%.

2. Results and Discussion

2.1. Structure Analysis

The representative X-ray diffraction (XRD) patterns of MTO:*x* Cr^{3+} (*x* = 0–0.06) were monitored and analyzed by the Rietveld refinements to confirm the phase purity and crystal structures (**Figure 1**a,b; Figure S1, Supporting Information). The diffraction peaks can be accurately assigned to $Mg_4Ta_2O_9$ (PDF#38-1458), though several diffraction peaks of the impurity phase $MgTa_2O_6$ (denoted by a star) also appeared. The comparison of the emission of MTO:0.03 Cr^{3+} with that of $MgTa_2O_6$: 0.03 Cr^{3+} as well as the photos of the above two samples are shown in Figure S2 (Supporting Information), and the results indicate that the existent impurity phase has no significant influence on the luminescence properties of MTO:Cr^{3+}. The corresponding refinement results are summarized in Tables S1, S2 (Supporting Information), and the acceptable *R*-factors confirm the reliability of the refinements. MTO crystallizes in a hexagonal structure with a space group of $p\bar{3}c1$ (165). According to the above results, the lattice parameters and the cell volumes show a decreasing trend with Cr^{3+} concentration because the smaller Cr^{3+} (r = 0.62 Å, coordination number (CN) = 6) substitutes the larger Mg^{2+} (r = 0.72 Å, CN = 6) or Ta^{5+} (r = 0.64 Å, CN = 6), which leads to the lattice shrinkage.[29–31] As depicted in Figure 1c, in the unit cell of MTO, two cations of Mg and Ta are in the form of (MgO_6) and (TaO_6) octahedral by sharing corner oxygens.[32–37] Generally, both the octahedral sites of Mg^{2+} and Ta^{5+} can expect to be occupied by Cr^{3+} with $3d^3$ orbitals due to the similar ionic radius, but considering the different valence states, we designed that Cr^{3+} ions only substitute Mg^{2+} sites while equal concentration of Li^+ ions was introduced into MTO to substitute Mg^{2+} for the valence balance, additionally, a second low-temperature sintering step under reducing atmosphere was also utilized to avoid Cr^{3+} being oxidized into Cr^{6+}.[16] The electron paramagnetic resonance (EPR) spectrum was also given to probe the local site symmetry of Cr^{3+}. As shown in Figure 1d, the EPR spectrum of MTO:0.03 Cr^{3+} contains two kinds of signals at *g* values of 3.68 and 1.98, respectively. The signal at g = 3.68 is attributed to the isolated Cr^{3+} ions, and several signals are observed for the isolated Cr^{3+} ions, indicating the existence of several types of Cr^{3+} sites. The weak but broad signal at g = 1.98 is assigned to the exchange coupled Cr^{3+} pairs, which reflects a disturbance environment of Cr^{3+}-Cr^{3+} pairs.[10,38] Moreover, according to the refinement results, the average isotropic displacement parameters length of the Mg—O bond dramatically decreases with Cr^{3+} content, but that of the Ta—O bond keeps almost unchanged, demonstrating that the Cr^{3+} ions mainly enter into the Mg^{2+} site. Similar results have been proved in other materials.[32,39]

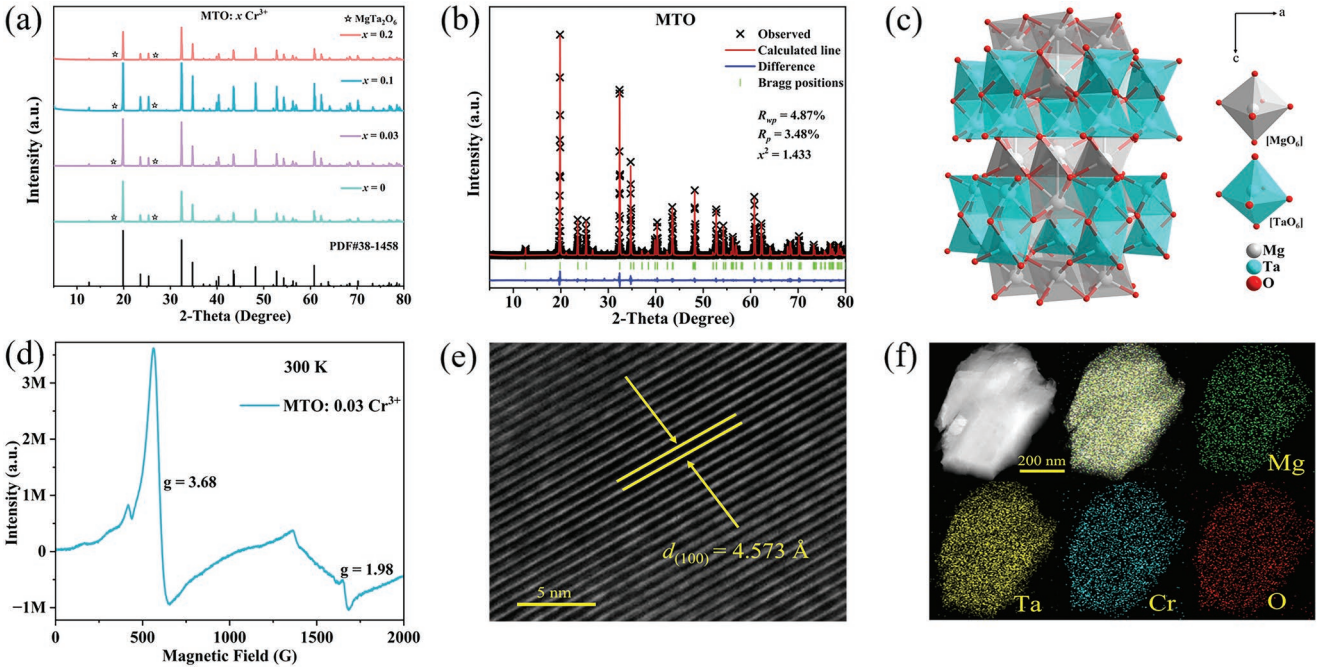

Figure 1. a) XRD patterns of MTO:*x* Cr^{3+} (*x* = 0–0.2); b) Rietveld refinement XRD of MTO; The crystal structure and the coordination environments (c), EPR spectrum (d), HRTEM images (e) as well as morphology and mapping (f) of MTO:0.03 Cr^{3+}.

As shown in Figure 1e, a large number of lattice fringes can be clearly observed in a high-resolution transmission electron microscopy (HRTEM) image, indicating the high crystallinity of MTO:0.03 Cr^{3+}. The d-spacing value of the (100) plane is measured as 4.573 Å, which is consistent well with its theoretical value of 4.470 Å. An energy dispersive spectrometer (EDS) was utilized to analyze the chemical composition and the relevant results are shown in Figure S3 and Table S3 (Supporting Information). In Figure 1f, the elemental mapping results depict that Mg, Ta, Cr, and O were uniformly distributed throughout the MTO:0.03 Cr^{3+} sample.

2.2. Photoluminescence Properties

Figure 2a depicts the excitation and emission spectra of MTO:0.03 Cr^{3+} at room temperature. Under 450 nm excitation, MTO:0.03 Cr^{3+} exhibits a single broadband NIR emission peaking at 850 nm with an FWHM of 188 nm (2502 cm^{-1}), attributing to spin-allowed d-d ($^4T_2 \rightarrow {}^4A_2$) transition of Cr^{3+} in a weak octahedral environment.[40] The corresponding excitation spectrum (λ_{em} = 850 nm) includes two excitation bands at 460 and 680 nm, originating from $^4A_2 \rightarrow {}^4T_1$ and $^4A_2 \rightarrow {}^4T_2$ transitions of Cr^{3+}, respectively.[41] The blue excitation band as well as the NIR emission band indicate the potential for NIR pc-LED. Additionally, the Tanabe–Sugano diagram is given in Figure S4a (Supporting Information) to clearly understand the crystal field strength of octahedrally coordinated Cr^{3+} in the MTO host. The crystal field strength and Racah parameters, *Dq* and *B*, were calculated and the results are shown in Supporting Information. The ratio of *Dq*/*B* is calculated to be 1.91, confirming that Cr^{3+} ions are in a weak crystal field site with a $^4T_2$ state lowering than that of ^2E, and thus only the broadband emission ascribed to the $^4T_2 \rightarrow {}^4A_2$ transition of Cr^{3+} can be detected. The weak crystal field of Cr^{3+} in MTO can also be demonstrated by the only dominated broad $^4T_2 \rightarrow {}^4A_2$ band at 77 K (Figure S4b, Supporting Information). To optimize the proper doping site of Cr^{3+}, the comparison of the emission spectra between Cr^{3+} ions only substitute Mg^{2+} and Cr^{3+} ions simultaneously substitute Mg^{2+} and Ta^{5+} ($Mg_{3.98}Ta_{1.99}O_9$: 0.03 Cr^{3+}) are given in Figure S5 (Supporting Information), the higher emission intensity further indicates that Cr^{3+} ions prefer to substitute Mg^{2+} ions.

Various Cr^{3+} doped MTO phosphors were synthesized to demonstrate the luminescence properties and the corresponding emission spectra were also recorded. As depicted in Figure 2b, under 450 nm excitation, the peak position shifts from 839 nm (x = 0.005) to 892 nm (x = 0.2) while the corresponding FWHM increases from 173 nm (2394 cm^{-1}) to 229 nm (2807 cm^{-1}), which may cause by the multiple octahedral environments of Cr^{3+} in MTO and the energy transfer among Cr^{3+} ions at high doping level. In Figure 2c, the emission intensity reaches the maximum when x is 0.03, after that it decreases gradually due to the well-known concentration quenching effect.[42] The corresponding excitation spectra as

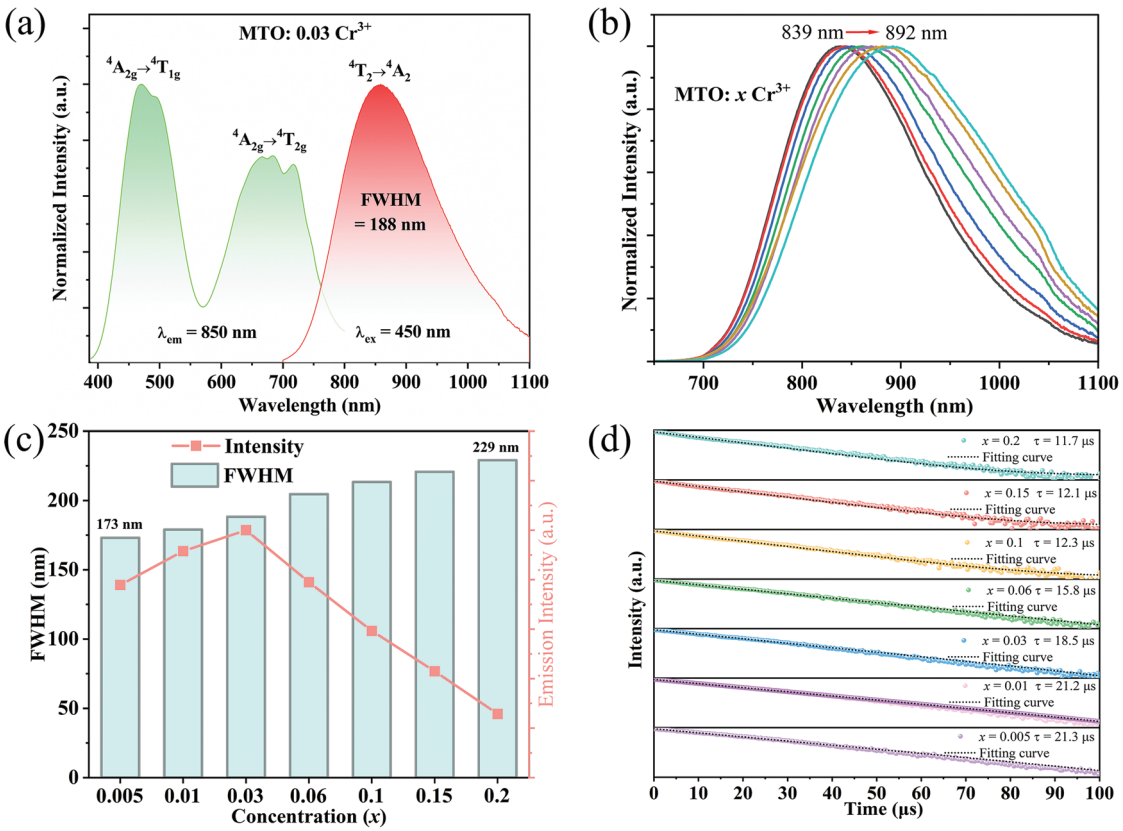

Figure 2. a) The room temperature excitation and emission spectra of MTO:0.03 Cr^{3+}; b) The normalized emission spectra and c) the FWHM and emission intensities of MTO:*x* Cr^{3+} under 450 nm excitation; d) Fluorescence decay curves of Cr^{3+} in MTO:*x* Cr^{3+} (excited at 460 nm, monitored at 850 nm).

Table 1. λ_{em}, FWHM, IQE, Abs, EQE, NIR output power and photoelectric efficiency of MTO:0.03 Cr^{3+} and some reported phosphors.

Samples	λ_{em} [nm]	FWHM [nm]	IQE [%]	Abs [%]	EQE [%]	NIR output power	Photoelectric efficiency	Ref.
MTO:0.03 Cr^{3+}	850	188	72	46.4	33.4	60.9 mW@150 mA	22.1%@10mA	This work
$GaTaO_4$:0.006 Cr^{3+}	840	140	91.2	34.3	31.3	178 mW@500 mA	6%@500 mA	[44]
$LiInSi_2O_6$:6% Cr^{3+}	840	143	75	\	\	51.6 mW@100 mA	17.8%@100 mA	[45]
$LiGaP_2O_7$:12% Cr^{3+}	846	170	47.8	59.2	28.3	28.1 mW@120 mA	7.8%@120 mA	[46]
$LaSc_{2.4}Ga_{0.6}B_4O_{12}$:0.07 Cr^{3+}	850	\	52.1		\	\	\	[47]
$Sr_9Ga(PO_4)_7$:0.8 Cr^{3+}	850	\	66.3	45.1	29.9	19.79 mW@150 mA	12.3%@20 mA	[48]
$(Mg_{0.6}Li_{0.4})(Mg_{0.6}Sc_{0.4})Ge_2O_6$:4% Cr^{3+}	874	182	66.6	47.3	31.5	\	\	[49]
$LiScP_2O_7$:0.06 Cr^{3+}	880	170	38	53	20	19 mW@100 mA	7%@100 mA	[50]
$LiInGe_2O_6$:8% Cr^{3+}	880	172	81.2	49.0	39.8	\	\	[51]
Sr_2ScSbO_6:3% Cr^{3+}	890	130	82.0	43.5	35.7	\	\	[52]
$NaScGe_2O_6$:0.03 Cr^{3+}	895	162	40.2	\	\	7.283 mW@150 mA	1.7%@150 mA	[53]
$NaInGe_2O_6$:0.07 Cr^{3+}	900	175	34	\	\	25.2 mW@120 mA	8.2%@20 mA	[54]
$Mg_3Ga_{1.9}In_{0.1}GeO_8$:0.03 Cr^{3+}	910	244	\	\	\	6.1 mW@60 mA	8.5%@60 mA	[55]
$CaScAlSiO_6$:0.5% Cr^{3+}	925	215	23	\	\	\	\	[56]
$Cs_2AgInCl_6$:0.1 Cr^{3+}	1010	180	22.0	\	\	\	\	[57]

well as the diffuse reflection (DR) spectra were also shown in Figure S6a,b (Supporting Information), and the obvious reflection bands correspond well with the found in the excitation spectrum. The room temperature fluorescence decay curves of MTO:x Cr^{3+} monitored at 850 nm are shown in Figure 2d. The decay curves can be well fitted by the single exponential profile, and the lifetime of Cr^{3+} monotonically decreases with the increase of the concentration, which also demonstrates the energy transfer among Cr^{3+} ions.[43]

The IQE and EQE are key parameters directly determining the possibility of phosphors for LED application. The QE of MTO:0.03 Cr^{3+} was measured and the corresponding spectrum was shown in Figure S7 (Supporting Information). The IQE value of MTO:0.03 Cr^{3+} under 460 nm excitation was measured to be 72% while the Abs is 46.4%, resulting in an EQE value of 33.4%. The Abs of MTO:0.03 Cr^{3+} with perovskite-like structure is higher than that of most Cr^{3+}-activated phosphor with garnet structure, and its EQE is also higher than most of the multi-site Cr^{3+}-activated systems with peak emission wavelength >850 nm (see **Table 1** for detailed comparison).

2.3. Photoluminescence Thermal Stability

Since the generated heat of LED chips and stokes loss of phosphors will decrease the emission intensity, thermal quenching is another key assessment index for phosphors. To give insight into the thermal quenching behavior of MTO:0.03 Cr^{3+}, the temperature-dependent emission spectra were further investigated in **Figure 3**. The emission intensity of MTO:0.03 Cr^{3+} experiences a continuous reduction, and still keeps 58.4% of its initial value as the temperature is elevated from 30 °C to 100 °C. Additionally, the FWHM of the NIR emission increases from 188 nm (2502 cm^{-1}) at 30 °C to 240 nm (3323 cm^{-1}) at 300 °C, which may attribute to the increased electron-phonon interaction.[58] To clearly understand the thermal quenching behavior, the activation energy ΔE_a of MTO:0.03 Cr^{3+} was calculated based on the Arrhenius formula and given in Figure S8 (Supporting Information). ΔE_a is determined to be 0.345 eV, which is larger than most Cr^{3+}-activated longer wavelength emission NIR phosphors (Table 1), indicating the good thermal stability of MTO:0.03 Cr^{3+}.

2.4. Photoelectric Performance and Applications of NIR LEDs

To prove the application potential of MTO:Cr^{3+}, a NIR pc-LED was fabricated by combining a 460 nm LED chip with the optimized MTO:0.03 Cr^{3+}, and a home-made testing system was also designed, as simplified in **Figure 4**a. Figure 4b shows the photographs of the lightened device. The electroluminescence spectrum contains a broadband NIR emission peaking at 850 nm and a narrow blue emission at 460 nm (Figure 4c). The driven current-dependent NIR light output power and photoelectric efficiency of the NIR pc-LED device are also given in Figure 4d. The NIR light output power increases from 5.7 mW (10 mA) to 60.9 mW (150 mA). Additionally, the NIR photoelectric efficiencies are calculated to be 22.1% and 14.1% at 10 and 150 mA, respectively, which are higher than that of the most reported NIR pc-LEDs with peak emission wavelength >850 nm (see Table 1). The "efficiency droop" of the blue LED chip mainly results in the above decrease in photoelectric efficiency (see Figure S9, Supporting Information).[59,60] Figure 4e shows the normalized emission spectra of the fabricated NIR pc-LED (0.5 W) via the light penetrating the thin apple slices. The absorption in the range of 900–1050 nm is assigned to the O-H chemical group of the apple, and it can be obtained by the comparison of the measured emission spectra with and without apple slices.[61] The emission intensity decreases with the increase of the thickness of the apple slices, and when the

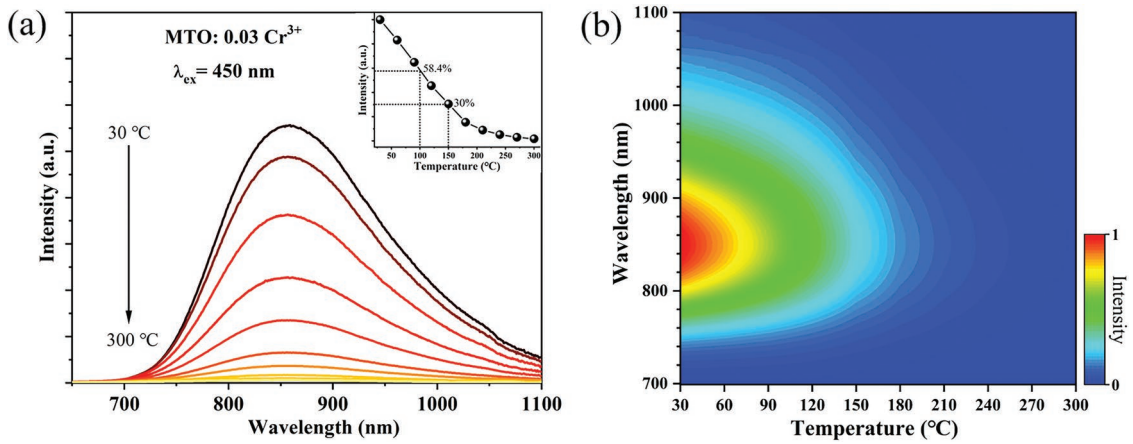

Figure 3. a) Temperature-dependent emission spectra and emission intensities of MTO:0.03 Cr^{3+} recorded upon excitation at 450 nm in the temperature range from 30 °C to 300°C; b) The corresponding contour plot of the emission spectra (*y*-axis) and temperature (*x*-axis) for MTO:0.03 Cr^{3+}.

thickness is 12 mm, the detector can also clearly detect the signal. The superior performance of the LED device indicates the application potential of MTO:Cr^{3+} as an NIR light source.

3. Conclusion

In summary, a series of MTO:*x* Cr^{3+} (*x* = 0.005–0.2) phosphors were successfully synthesized by high-temperature solid-state reactions. As a result of both synthesis strategy and the unique crystal structure of the host lattice MTO, a high IQE and Abs of 72% and 46.4% were achieved. MTO:Cr^{3+} performs a broadband NIR emission in the whole 700–1100 nm region with the peak located at 850 nm and FWHM of 188 nm. In addition, the NIR pc-LEDs prepared using the developed phosphors have excellent optical properties, high NIR output power (5.7 mW@10 mA), and high photoelectric efficiency (22.1%@10 mA). Our results provide a promising NIR

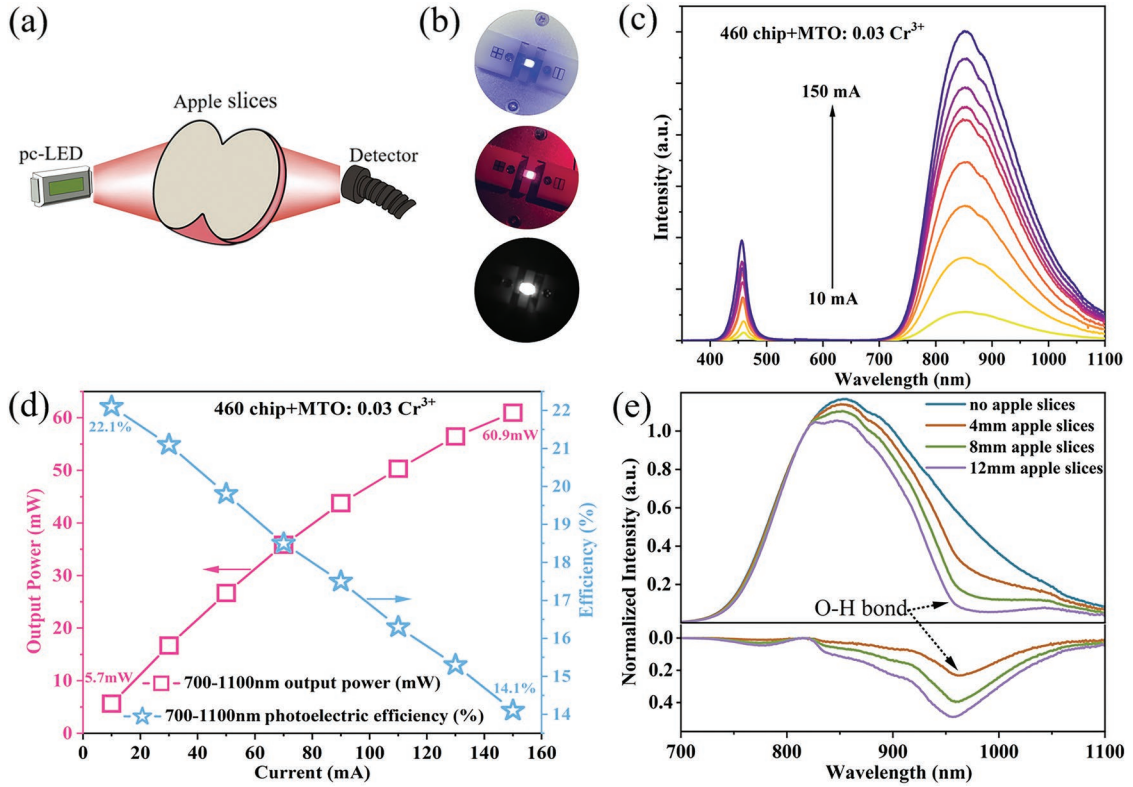

Figure 4. a) Schematic diagram of experimental equipment; b) Photographs of lightened pc-LED without and with a long pass filter at 650 nm; c) Electroluminescence spectrum of the device under the current ranges from 10 to 150 mA; d) Driven current dependent NIR light output power and photoelectric efficiency of the fabricated NIR pc-LED; e) The normalized emission spectra obtained by irradiating the apple slices with the fabricated NIR pc-LED.

phosphor for NIR light sources with broad commercial application prospects.

4. Experimental Section

Synthesis: A series of samples of MTO:x Cr^{3+} (x = 0.005–0.2) were prepared by high-temperature solid-state reaction. MgO (99.99%), Ta_2O_5 (99.99%), and Cr_2O_3 (99.999%) were selected as raw materials and weighted in stoichiometric ratios. Li^+ was also used as the charge compensation for the substitution of Mg^{2+} by Cr^{3+}, and 100% excess of Li_2CO_3 was added for the evaporation loss during the sintered process. The raw materials were ground in an agate mortar and then transferred into a corundum crucible. The resulting mixtures were sintered in air at 1550 °C for 6 h and subsequently sintered under a reducing atmosphere (95% N_2-5% H_2) at 1400 °C for 4 hours to obtain the final powders. The NIR pc-LED was fabricated by encapsulating the prepared MTO:0.03 Cr^{3+} onto a blue LED chip (460 nm, 0.5 W, SMD 5730 PCB), where the mass ratio of MTO:0.03 Cr^{3+} to the transparent silicone was fixed at 1:1.

Characterization: XRD patterns were determined by a Rigaku diffractometer (Ultima-IV, with Cu Kα radiation) in the 2θ range from 5° to 120°. The Rietveld refinement analysis was performed on the general structure analysis system program by using $Mg_4Ta_2O_9$ (PDF#38-1458) as a starting model. The HRTEM (JEM-2100F, JEOL) with an EDS was used to characterize the microstructure and the compositions of the samples. The room temperature excitation and emission spectra, temperature-dependent emission spectra as well as the photoelectric properties of the fabricated NIR pc-LEDs device were given by LHS-1000 (EVERFINE) equipped with an array spectrophotometer (HAAS-2000), where the temperature was controlled by a temperature controller (TAP-02, Orient KOJI). The room temperature emission intensities were obtained by using HITACHI F-7000. The excitation and emission spectra at 77 K were measured by FLS980 (Edinburgh Instruments). A UV–VIS–NIR spectrometer (UV3600, Shimadzu) was used to obtain the DR spectra. The EPR measurement at room temperature was performed by Bruker (A300). The fluorescence decays of Cr^{3+} were determined by an FS5 fluorimeter (Edinburgh Instruments) (the excitation source was a 450 nm laser diode). The IQE and absorption were recorded by a quantum yield measurement system (Quantaurus-QY Plus C13534-12, Hamamatsu Photonics).

Supporting Information

Supporting Information is available from the Wiley Online Library or from the author.

Acknowledgements

This work was partially supported by the National Natural Science Foundation of China (Grant No. 11904186; 12104231), the Research Program of Science and Technology at Universities of Inner Mongolia (Grant No. NJZZ20001), the Natural Science Foundation of Jiangsu Province (BK20200783).

Conflict of Interest

The authors declare no conflict of interest.

Data Availability Statement

The data that support the findings of this study are available from the corresponding author upon reasonable request.

Keywords

850 nm emission, broadband emission, Cr^{3+} doping, near-infrared light sources, perovskite-like structures

Received: September 22, 2022
Revised: November 20, 2022
Published online:

[1] C. Wu, Y. Wu, X. Zhu, J. Zhang, J. Liu, Y. Zhang, *Nano Today* **2021**, *36*, 100963.
[2] Y. Liu, S. He, D. Wu, X. Dong, W. Zhou, *ACS Appl. Electron. Mater.* **2022**, *4*, 643.
[3] H. Cai, S. Liu, Z. Song, Q. Liu, *J. Mater. Chem. C* **2021**, *9*, 5469.
[4] J. Wu, W. Zhuang, R. Liu, Y. Liu, T. Gao, C. Yan, M. Cao, J. Tian, X. Chen, *J. Rare Earth* **2021**, *39*, 269.
[5] D. Huang, H. Zhu, Z. Deng, H. Yang, J. Hu, S. Liang, D. Chen, E. Ma, W. Guo, *J. Mater. Chem. C* **2021**, *9*, 164.
[6] J. Zhong, Y. Zhuo, F. Du, H. Zhang, W. Zhao, J. Brgoch, *ACS Appl. Mater. Interfaces* **2021**, *13*, 31835.
[7] H. Xu, G. Bai, K. He, S. Tao, Z. Lu, Y. Zhang, S. Xu, *Mater. Today Phys.* **2022**, *28*, 100872.
[8] L. Zhou, Z. Lyu, D. Sun, S. Shen, T. Tan, L. Wang, H. Zhao, H. You, *Adv. Opt. Mater.* **2022**, *10*, 2201308.
[9] R. Y. Li, Y. F. Liu, C. X. Yuan, G. Leniec, L. J. Miao, P. Sun, Z. H. Liu, Z. H. Luo, R. Dong, J. Jiang, *Adv. Opt. Mater.* **2021**, *9*, 2100388.
[10] H. Zeng, T. Zhou, L. Wang, R.-J. Xie, *Chem. Mater.* **2019**, *31*, 5245.
[11] H. Zhang, J. Zhong, C. Li, L. Wang, W. Zhao, *J. Lumin.* **2022**, *251*, 119211.
[12] S. Miao, Y. Liang, Y. Zhang, D. Chen, X. J. Wang, *ACS Appl. Mater. Interfaces* **2021**, *13*, 36011.
[13] L. Zhang, D. Wang, Z. Hao, X. Zhang, G. h. Pan, H. Wu, J. Zhang, *Adv. Opt. Mater.* **2019**, *7*, 1900185.
[14] H. Zhang, J. Zhong, F. Du, L. Chen, X. Zhang, Z. Mu, W. Zhao, *ACS Appl. Mater. Interfaces* **2022**, *14*, 11663.
[15] Q. Zhang, G. Li, P. Dang, D. Liu, D. Huang, H. Lian, J. Lin, *J. Mater. Chem. C* **2021**, *9*, 4815.
[16] J. Qiao, G. Zhou, Y. Zhou, Q. Zhang, Z. Xia, *Nat. Commun.* **2019**, *10*, 5267.
[17] J. J. Joos, D. Van der Heggen, L. Martin, L. Amidani, P. F. Smet, Z. Barandiaran, L. Seijo, *Nat. Commun.* **2020**, *11*, 3647.
[18] Y. Xiao, W. Xiao, D. Wu, L. Guan, M. Luo, L. D. Sun, *Adv. Funct. Mater.* **2022**, *32*, 2109618.
[19] Z. Wu, X. Han, J. Wang, Y. Zhou, K. Xing, S. Cao, J. Zhao, B. Zou, R. Zeng, *J. Mater. Chem. C* **2022**, *10*, 10292.
[20] Q. Zhang, D. Liu, P. Dang, H. Lian, G. Li, J. Lin, *Laser Photonics Rev.* **2022**, *16*, 2100459.
[21] E. Song, H. Ming, Y. Zhou, F. He, J. Wu, Z. Xia, Q. Zhang, *Laser Photonics Rev.* **2021**, *15*, 2000410.
[22] G. Zheng, W. Xiao, J. Wu, X. Liu, H. Masai, J. Qiu, *Adv. Sci.* **2022**, *9*, 2105713.
[23] M.-H. Fang, G. N. A. De Guzman, Z. Bao, N. Majewska, S. Mahlik, M. Grinberg, G. Leniec, S. M. Kaczmarek, C.-W. Yang, K.-M. Lu, H.-S. Sheu, S.-F. Hu, R.-S. Liu, *J. Mater. Chem. C* **2020**, *8*, 11013.
[24] B. Malysa, A. Meijerink, T. Jüstel, *J. Lumin.* **2016**, *171*, 246.
[25] S. Liu, Z. Wang, H. Cai, Z. Song, Q. Liu, *Inorg. Chem. Front.* **2020**, *7*, 1467.
[26] V. Rajendran, M.-H. Fang, G. N. D. Guzman, T. Lesniewski, S. Mahlik, M. Grinberg, G. Leniec, S. M. Kaczmarek, Y.-S. Lin, K.-M. Lu, C.-M. Lin, H. Chang, S.-F. Hu, R.-S. Liu, *ACS Energy Lett.* **2018**, *3*, 2679.
[27] S. He, P. Li, Y. Ren, G. Wei, Y. Wang, Y. Yang, R. Li, J. Li, Y. Shi, X. Shi, Z. Wang, *Inorg. Chem.* **2022**, *61*, 11284.

[28] D. Liu, G. Li, P. Dang, Q. Zhang, Y. Wei, H. Lian, M. Shang, C. C. Lin, J. Lin, *Angew. Chem., Int. Ed.* **2021**, *60*, 14644.
[29] Y. Liu, J. Gao, W. Shi, X. Feng, Z. Zhou, J. Wang, J. Guo, R. Kang, B. Deng, R. Yu, *Ceram. Int.* **2021**, *47*, 18814.
[30] H. Cai, H. Chen, H. Zhou, J. Zhao, Z. Song, Q. L. Liu, *Mater. Today Chem.* **2021**, *22*, 100555.
[31] D. Liu, G. Li, P. Dang, Q. Zhang, Y. Wei, L. Qiu, M. S. Molokeev, H. Lian, M. Shang, J. Lin, *Light: Sci. Appl.* **2022**, *11*, 112.
[32] G. Liu, M. S. Molokeev, B. Lei, Z. Xia, *J. Mater. Chem. C* **2020**, *8*, 9322.
[33] H. Suo, Y. Wang, X. Zhao, X. Zhang, L. Li, K. Guan, W. Ding, P. Li, Z. Wang, F. Wang, *Laser Photonics Rev.* **2022**, *16*, 2200012.
[34] L. Lou, S. Zhao, S. Yuan, D. Zhu, F. Wu, Z. Mu, *Inorg. Chem. Front.* **2022**, *9*, 3522.
[35] R. E. Newnham, J. F. Dorrian, E. P. Meagher, *Mater. Res. Bull.* **1970**, *5*, 199.
[36] A. J. Brown, J. Liu, F. P. Marlton, M. Avdeev, B. J. Kennedy, C. D. Ling, *J. Solid State Chem.* **2020**, *287*, 121385.
[37] R. Mani, N. S. P. Bhuvanesh, K. V. Ramanujachary, W. Green, S. E. Lofland, J. Gopalakrishnan, *J. Mater. Chem.* **2007**, *17*, 1589.
[38] Z. Jia, C. Yuan, Y. Liu, X. J. Wang, P. Sun, L. Wang, H. Jiang, J. Jiang, *Light: Sci. Appl.* **2020**, *9*, 86.
[39] M. Mao, T. Zhou, H. Zeng, L. Wang, F. Huang, X. Tang, R.-J. Xie, *J. Mater. Chem. C* **2020**, *8*, 1981.
[40] E. T. Basore, W. Xiao, X. Liu, J. Wu, J. Qiu, *Adv. Opt. Mater.* **2020**, *8*, 2000296.
[41] L. Zhang, S. Zhang, Z. Hao, X. Zhang, G.-h. Pan, Y. Luo, H. Wu, J. Zhang, *J. Mater. Chem. C* **2018**, *6*, 4967.
[42] D. Wu, H. Wu, Y. Xiao, X. Dong, Y. Wang, W. Zhou, Y. Liu, L. Zhang, *J. Lumin.* **2022**, *244*, 118750.
[43] Y. Zhang, S. Miao, Y. Liang, C. Liang, D. Chen, X. Shan, K. Sun, X. J. Wang, *Light: Sci. Appl.* **2022**, *11*, 136.
[44] J. Zhong, Y. Zhuo, F. Du, H. Zhang, W. Zhao, S. You, J. Brgoch, *Adv. Opt. Mater.* **2022**, *10*, 2101800.
[45] X. Xu, Q. Shao, L. Yao, Y. Dong, J. Jiang, *Chem. Eng. J.* **2020**, *383*, 123108.
[46] C. Yuan, R. Li, Y. Liu, L. Zhang, J. Zhang, G. Leniec, P. Sun, Z. Liu, Z. Luo, R. Dong, J. Jiang, *Laser Photonics Rev.* **2021**, *15*, 2100227.
[47] T. Gao, W. Zhuang, R. Liu, Y. Liu, C. Yan, X. Chen, *Cryst. Growth Des.* **2020**, *20*, 3851.
[48] F. Zhao, H. Cai, Z. Song, Q. Liu, *Chem. Mater.* **2021**, *33*, 3621.
[49] H. Liu, F. Zhao, H. Cai, Z. Song, Q. Liu, *J. Mater. Chem. C* **2022**, *10*, 9232.
[50] L. Yao, Q. Shao, S. Han, C. Liang, J. He, J. Jian, *Chem. Mater.* **2020**, *32*, 2430.
[51] T. Liu, H. Cai, N. Mao, Z. Song, Q. Liu, *J. Am. Ceram. Soc.* **2021**, *104*, 4577.
[52] M. Zhao, S. Liu, H. Cai, F. Zhao, Z. Song, Q. Liu, *Sci. China Mater.* **2022**, *65*, 748.
[53] X. Zhou, W. Geng, J. Li, Y. Wang, J. Ding, Y. Wang, *Adv. Opt. Mater.* **2020**, *8*, 1902003.
[54] W. Zhou, J. Luo, J. Fan, H. Pan, S. Zeng, L. Zhou, Q. Pang, X. Zhang, *Ceram. Int.* **2021**, *47*, 25343.
[55] D. Dai, Z. Wang, Z. Xing, X. Li, C. Liu, L. Zhang, Z. Yang, P. Li, *J. Alloys Compd.* **2019**, *806*, 926.
[56] D. Wen, H. Liu, Y. Guo, Q. Zeng, M. Wu, R. S. Liu, *Angew. Chem., Int. Ed.* **2022**, *61*, e202204411.
[57] F. Zhao, Z. Song, J. Zhao, Q. Liu, *Inorg. Chem. Front.* **2019**, *6*, 3621.
[58] T. Senden, R. J. A. van Dijk-Moes, A. Meijerink, *Light: Sci. Appl.* **2018**, *7*, 8.
[59] G. Zheng, W. Xiao, H. Wu, J. Wu, X. Liu, J. Qiu, *Laser Photonics Rev.* **2021**, *15*, 2100060.
[60] F. He, E. Song, H. Chang, Y. Zhou, Z. Xia, Q. Zhang, *ACS Appl. Mater. Interfaces* **2022**, *14*, 31035.
[61] T. Ma, X. Li, T. Inagaki, H. Yang, S. Tsuchikawa, *J. Food Eng.* **2018**, *224*, 53.